Extreme dust storm over the eastern Mediterranean in September 2015: Satellite, lidar, and surface observations in the Cyprus region

Rodanthi-Elisavet Mamouri[1,2], Albert Ansmann[3], Argyro Nisantzi[1], Stavros Solomos[2], George Kallos[4], and Diofantos G. Hadjimitsis[1]

[1]Cyprus University of Technology, Department of Civil Engineering and Geomatics, Limassol, Cyprus
[2]National Observatory of Athens, Athens, Greece
[3]Leibniz Institute for Tropospheric Research, Leipzig, Germany
[4]University of Athens, School of Physics, Division of Environment and Meteorology, Athens, Greece

Correspondence to: R.-E. Mamouri (rodanthi.mamouri@cut.ac.cy)

Abstract. A record-breaking dust storm originating from desert regions in northern Syria and Iraq occurred over the Eastern Mediterranean in September 2015. In this contribution of a series of two articles (part 1, observations, part 2, atmospheric modeling), we provide a comprehensive overview about the aerosol conditions during this extreme dust outbreak in the Cyprus region based on satellite observations (MODIS, aerosol optical thickness AOT, Ångström exponent), surface particle mass (PM_{10}) concentrations measured at four sites in Cyprus, visibility observations at three airports in southern Cyprus and corresponding conversion products (particle extinction coefficient, dust mass concentrations), and EARLINET lidar observations of dust vertical layering over Limassol, particle optical properties (backscatter, extinction, lidar ratio, linear depolarization ratio), and derived profiles of dust mass concentrations. Maximum 550 nm AOT was clearly >5 and correspondingly the mass loads were probably >10 g/m^2 over Larnaca and Limassol during the passage of an extremely dense dust front on 8 September 2015. Hourly mean PM_{10} values were close 8000 μg/m^3, the observed meteorological optical range (visibility) reduced to 300–750 m at Larnaca and Limassol. The visibility observations suggest peak values of the near-surface total-suspended-particle (TSP) extinction coefficients of 6000 Mm^{-1} and thus TSP mass concentrations of 10000 μg/m^3. The Raman/polarization lidar observations showed a two–layer structure of the dust plumes (reaching to about 4 km height), pointing to at least two different dust source regions. Dust particle extinction coefficients (532 nm) exceeded 1000 Mm^{-1} and the mass concentrations reached 2000 μg/m^3, respectively, in the elevated dust layers on 7 September, more than 12 hours before the peak dust front on 8 September reached the Limassol lidar station around local noon. Typical Middle East dust lidar ratios around 40 sr were observed in the dense dust plumes. The particle depolarization ratio decreased from around 0.3 in the lofted dust layers towards 0.2 at the end of the dust period (11 September) indicating an increasing impact of anthropogenic haze.

1 Introduction

On 7–11 September 2015, a record-breaking dust storm hit Cyprus. The visibility decreased to 300–500 m for more than 12 hours at Larnaca International Airport on 8 September, and the maximum aerosol optical thickness (AOT) exceeded >5 at 500 nm over eastern and southern Cyprus. The dense dust clouds with peak mass concentrations of the order of 10 mg/m^3

originated from Middle East deserts, mainly from northeastern Syria and northern Iraq. According to a recently presented climatology of strong and extreme dust events over the Mediterranean Sea (Gkikas et al., 2016), based on satellite observations from 2000–2013, extreme dust events, characterized by an AOT exceeding the climatological mean AOT by four standard deviations, occur, on average, 1-2 per year for a given site. In fact, eight extreme dust outbreaks (with AOT$>$0.75 at 500 nm) were observed at the Aerosol Robotic Network (AERONET) station at Limassol, Cyprus, in the Eastern Mediterranean in the time period from June 2011 to June 2015. However, extreme events with AOT$>$4.0 to 5.0 as in September 2015 are rather seldom and may occur once in a decade. An extended aerosol characteristics for the Mediterranean region, including statistics on strong dust events and an extended literature survey is given by Georgoulias et al. (2016).

Dust transport models widely failed to predict this record-breaking dust storm (http://sds-was.aemet.es/forecast-products/dust-forecasts/compared-dust-forecasts). This fact and the enormous dust mass concentrations measured in Cyprus motivated us to investigate the underlying weather conditions that caused this huge dust outbreak. Extreme dust events provide a unique opportunity to learn more about known and established dust mobilizing mechanisms and to identify and explore even new or not well parameterized dust emission processes. The dust storm was obviously linked to an extraordinary weather situation with dust mobilization features on scales which were too small to be resolved by the used global and regional weather and dust transport models. We investigate this extreme dust event in detail by combining the available dust observations in the Cyprus area (presented in this article) with complex atmospheric modeling (presented in the second paper, Solomos et al., Extreme dust storm over Middle-East and the eastern Mediterranean in September 2015: Modeling study with RAMS-ICLAMS, to be submitted to ACP). The occurrence of a haboob in northeastern Syria and northern Iraq was probably responsible for this unique dust outbreak. Haboobs are intense dust storms caused by strong thunderstorm activity, which are associated with density currents (Knippertz et al., 2007; Solomos et al., 2012), strong precipitation and vigorous cold-air downbursts reaching the ground and pushing huge amounts of dust and sand into the air.

The goal of this first article is to provide an overview of the available dust observations in the Cyprus region. We present time series of spaceborne observations (MODIS, Moderate Resolution Imaging Spectroradiometer) of aerosol optical thickness (AOT) for five sites in Cyprus, continuous particle mass concentration measurements (PM_{10}, mass concentration of particles with aerodynamic diameter smaller than 10 μm) at four stations, visibility observations from three airports in Cyprus, and lidar observations, performed at Limassol. We are not aware of any report in the literature in which a severe, record-breaking dust storm has been discussed in so much observational detail. The lidar measurements are especially highlighted in our study. The observed temporally and vertically resolved dust layering structures and the derived profiles of particle extinction coefficient and dust mass concentration provide indispensable information for dust transport simulation studies (presented in the second article). Comparison of modeled and lidar-derived dust profiles are of basic importance in model-based investigations of the relationship between given meteorological conditions over the dust source regions, dust mobilization, and observed long-range dust transport features (Heinold et al., 2009, 2011; Müller et al., 2009).

Several long-term lidar studies of dust outbreaks towards the Mediterranean are available, however with main focus on Saharan dust outbreaks (e.g. Amiridis et al., 2005; Mona et al., 2006, 2014; Papayannis et al., 2008; Papayannis et al., 2009). An extreme Saharan dust event with AOT up to 1.5 at 500 nm over southern Spain observed with lidar was discussed by

Guerrero-Rascado et al. (2009). A first lidar-based long-term study for the Eastern Mediterranean which includes Saharan as well as Middle East desert dust outbreaks has been presented by Nisantzi et al. (2015), based on the Limassol lidar observations.

After the introduction, a brief description of the observation methods, data analysis, and measurement products is given in Sect. 2. The observations are presented and in Sect. 3. A few concluding remarks are given in Sect. 4.

2 Aerosol instrumentation and observational products

2.1 EARLINET lidar profiling of dust optical properties and mass concentration

The lidar observations were conducted by the Cyprus University of Technology (CUT), at Limassol (34.7°N, 33°E, 23 m above sea level), Cyprus. The lidar station belongs to the European Aerosol Research Lidar Network (EARLINET) (Pappalardo et al., 2014) and is equipped with a 532 nm polarization/Raman lidar (nitrogen Raman channel at 607 nm)(Mamouri et al., 2013; Mamouri and Ansmann, 2014; Nisantzi et al., 2015). The EARLINET site is combined with an Aerosol Robotic Network (AERONET) station (Holben et al., 1998; Nisantzi et al., 2014, 2015) and located in the city center of Limassol (see CUT-TEPAK site in the AERONET data base, TEPAK stands for the greek name TEchologiko PAnepistimio Kyprou). Unfortunately, the CUT-TEPAK AERONET photometer was not available from July to October 2015 for calibration reasons.

Details of the lidar data analysis regarding the retrieval of the particle linear depolarization ratio δ, backscatter coefficient β, extinction coefficient σ, and extinction-to-backscatter ratio (lidar ratio) S, and of the separation of dust backscatter coefficient $\beta_{\rm d}$ and non-dust backscatter coefficient $\beta_{\rm nd}$ are given by Tesche et al. (2009a, b), Mamouri et al. (2012, 2013), and Mamouri and Ansmann (2014), and Nisantzi et al. (2014, 2015).

The dust mass concentrations $M_{\rm d}$ is then obtained from the backscatter coefficients $\beta_{\rm d}$ by means of the equation,

$$M_{\rm d} = \rho_{\rm d} c_{\rm v,d} \beta_{\rm d} S_{\rm d}\,, \tag{1}$$

with the dust particle density $\rho_{\rm d}$, assumed to be $2.6\,{\rm g/cm^{-3}}$ (Ansmann et al., 2012), the volume-to-extinction conversion factor $c_{\rm v,d} = v_{\rm d}/\sigma_{\rm d}$ with the dust volume concentration $v_{\rm d}$, and the dust lidar ratio $S_{\rm d}$.

By using a characteristic dust lidar ratio $S_{\rm d}$ (or even measured ones as during this dust storm), we convert the retrieved profiles of the backscatter coefficient $\beta_{\rm d}$ into respective profiles of dust extinction coefficient $\sigma_{\rm d}$. We use $S_{\rm d}$=40 sr for Middle East desert dust (Mamouri et al., 2013). Then, the dust extinction profile is converted into the particle volume and mass concentration profiles $v_{\rm d}$ and $M_{\rm d}$, respectively, by using conversion factors from AERONET column observations during pure desert dust situations. Appropriate conversion factors were derived from extended studies during large dust field campaigns in Morocco, Cabo Verde, and Barbados (Mamouri and Ansmann, 2016). The average conversion factor $c_{\rm v,d}$ is $0.64\pm0.06\times10^{-12}$Mm.

The uncertainties in all the optical properties, conversion factors and estimated microphysical properties are discussed by Tesche et al. (2009a); Ansmann et al. (2012), and Mamouri and Ansmann (2014). Relative uncertainties in the dust backscatter and extinction coefficients and lidar ratios are about 10–20% at dense dust conditions. Considering in addition a relative uncertainty of 10% in the assumed dust density $\rho_{\rm d}$ and of about 10% in the conversion factor $c_{\rm v,d}$, we yield an overall relative uncertainty of 20–30% in the estimated dust mass concentrations.

2.2 MODIS observations of AOT

MODIS (Moderate Resolution Imaging Spectroradiometer, MODIS, http://lance-modis.eosdis.nasa.gov/) products are used to describe the dust load in the Cyprus region. For five sites we calculated the mean AOT at 550 nm wavelength and mean Ångström exponent (for the 510–670 nm spectral range) from the available set of AOT data within areas with 50 km radius around these cities. The maximum retrievable AOT is 5.0. On 8 September, this value was frequently exceeded. The uncertainty in the retrieved AOT is $0.05 \pm 0.15 \times$ AOT (Levy et al., 2010, 2013).

2.3 PM_{10} observations of the Department of Labour Inspection of Cyprus

Non-validated hourly mean surface observations of PM_{10} concentrations are published by the Air Quality Department of Cyprus (Department of Labour Inspection, DLI, http://www.airquality.dli.mlsi.gov.cy/). We checked the uncertainty in the non-validated hourly values by comparing quality-assured 24-hour PM_{10} values (gravimetric method, European standard, kindly provided by DLI, personal communication, Chrysanthos Savvides) with respective 24-hour mean values calculated from the hourly mean non-validated data. We found deviations of ± 50 between the two daily means for the different sites of Larnaca, Limassol, and Pafos on 8 September 2015. The deviations reduced to about 20% later on (9–11 September).

2.4 Visibility observations of the Department of Meteorology of Cyprus

Another way to estimate the dust mass load at ground is based on observations of the so-called meteorological optical range (MOR) r_{vis} (better known as Koschmieder's visibility) (Koschmieder, 1924; Horvath and Noll, 1969; Horvath, 1971). We present visibility time series from three airports in Cyprus (Larnaca, Pafos, and Acrotiri, about 10 km southwest of the Limassol city center). The data are kindly provided by the Department of Meteorology, Cyprus (DoM, personal communication, Filippos Tymvios). The visibility values are estimated by human observers which are carefully trained after the guidelines of the World Meteorological Organization. The uncertainty of the MOR estimation is of the order of 20–30% for $r_{\mathrm{vis}} > 1000$ m up to 20 km. For lower MOR, the uncertainty may be considerably higher.

The visibility r_{vis} is linked to the particle extinction coefficient σ for 500–550 nm (in the visible wavelength spectrum) by the relationship (e.g., Horvath and Noll, 1969; Horvath, 1971)

$$\sigma = 3.0/r_{\mathrm{vis}} \times 10^6 \tag{2}$$

with r_{vis} in m and σ in Mm^{-1}. The AOT of 3.0 describes the attenuation of light along the horizontal distance with length r_{vis}. Eq. (2) is based on the original Koschmieder formula. Koschmieder (1924) used an AOT of 3.9 which causes an apparent contrast of the object against the bright background of 0.02. The AOT of 3.0 is related to the intuitive concept of visibility through the contrast threshold taken as 0.05.

Under clear-air conditions, the particle extinction coefficient at 500–550 nm is about 50–150 Mm^{-1}. MOR is then in the range of 20–50 km. In the Eastern Mediterranean around Cyprus, we may add a marine aerosol contribution to particle extinction by about 50–100 Mm^{-1} so that the visibility is usually between 10–30 km in the polluted marine environment. During

the strong dust outbreak in September 2015, however, the visibility dropped to values of the order of 300-1000 m, which corresponds to dust extinction coefficients of the order of 3000-10000 Mm^{-1}. At these conditions, contribution of marine and anthropogenic particles to the total particle extinction coefficient of the order of a few percent can be neglected.

In order to compare the visibility observations and in situ PM_{10} mass concentrations, we convert the derived particle extinction coefficients σ_d into dust mass concentrations M_d by using the relationship (compare Eq. (1))

$$M_\mathrm{d} = \rho_\mathrm{d} c_\mathrm{v,d} \sigma_\mathrm{d} \tag{3}$$

with the volume-to-extinction dust conversion factor $c_\mathrm{v,d}$ of $0.64 \pm 0.06 \times 10^{-12}$Mm and the dust particle density ρ_d of $2.6\,\mathrm{g/cm}^{-3}$, as introduced in Sect. 2.1. The uncertainty mainly depends on the uncertainty in the visibility estimation.

3 Results

3.1 Dust transport features: Horizontal and vertical dust distribution

Fig. 1 provides an overview about the enormous dust storm in the beginning of September 2015 as seen by MODIS. Optically dense dust plumes were advected from the east and reached Cyprus on 7 September 2015. Parts of the dust plumes were so dense that the dark surface of the Mediterranean Sea and eastern and southern parts of the island of Cyprus were no longer visible from space. The highest dust load was observed over Cyprus on 8 September 2015. On this day, the 550 nm AOT clearly exceeded 5 as will be discussed in detail in the next subsection. Unfortunatly, lidar observations were not possible on 8 September. The dust amount slowly decreased and showed a second, much weaker maximum on 10–11 September. The Troodos mountains (dark area in southwestern Cyprus) with top heights up to 2000 m were always visible during the dust storm (even on 8 September, AOT$>$5). This indicates that the thickest dust layers crossed Cyprus at heights below 1500 m height. This conclusion is supported by the lidar observations.

To provide a coarse idea information about the dust source regions and insight into the main airflow during this dust event, Fig. 2 shows six-day backward trajectories for 8 September 2015 (9 UTC) for arrival heights in the lower dust layer (reaching to about 1.5 km height according to the Limassol lidar observations on 7 and 9 September, also clearly visible in the Nicosia radiosonde profiles of temperature and relative humidity (RH)on 8 September, 6 and 12 UTC launches, as will be discussed below) and in the upper dust layer (from 1.5–3.8 km as indicated by the Nicosia temperature and RH profiles) over the Eastern Mediterranean at 34.7°N and 35°E, about 160 km east of Limassol. The HYSPLIT (HYbrid Single-Particle Lagrangian Integrated Trajectory, http://www.arl.noaa.gov/HYSPLIT.php) model was used for this purpose (Stein et al., 2015). Dust from Middle East deserts were transported to the northwest towards northern Iraq and northeastern Syria, and then to the west towards the Mediterranean Sea.

Figure 3 presents the Limassol lidar observations of the vertical dust layering observed from 7-11 September 2015. As mentioned, dust advection occurred in two pronounced, separated dust layers (the lower one up to 1.5–1.7 km, the upper one up to 3.5-4.2 km height) on 7-9 September. A first thick dust layer crossed Cyprus in the evening of 7 September between 2 and 3.7 km height. The detected two-layer structure prevailed on 8 September (no lidar observations to avoid any potential damage

of lidar optics and detection units). This is corroborated by the profiles of temperature and RH measured with radiosondes launched at Nicosia about 60 km northeast of Limassol at 6 and 12 UTC. The peak dust front reached Limassol between 8–9 UTC. The vertical gradients of temperature and RH were different in the two layers. Furthermore, the 12 UTC RH profile increased from values of 10–15% at the surface to about 30% at the top of the lower layer in 1.5 km height and indicated well-mixed dust conditions. Similarly, the potential temperature was almost height independent and thus also indicated favorable conditions for vertical mixing. In the upper layer from 1.5–3.8 km height, slightly stable conditions were observed.

Figure 4 depicts the two-layer dust structures in terms of dust mass concentration derived from the lidar observations in the evening of 7 September. The values exceeded already 2000 μg/m^3 below 1500 m height and 600 μg/m^3 around 3 km height on 7 September 2015. The two–layer structure of the dust plume is well reflected in the meteorological data measured with the Nicosia radiosonde on 8 September, 6 UTC, just before arrival of the main dust front. As mentioned above, the changes in RH and potential temperature with height indicated different air masses and thus different dust source regions above and below about 1500 m height. The meteorological data also indicate that the dust layer was still lofted (base height at around 700 m above ground) in the morning of 8 September, at 6 UTC.

The same two-layer structure was then observed again with lidar a day later on 9 September 2015 (see Figure 3), again in consistency with the temperature and humidity profiles of the Nicosia radiosonde. In the evening of 10 September, another elevated optically dense dust layer crossed the EARLINET lidar station. Finally, on 11 September, a more homogeneous and temporally constant layering was found. The main layer was now below 2000 m. Traces of dust were however detected up to 3000–4000 m height. On 12 September (not shown), a strong decrease in the AOT values indicated the end of the dust episode.

In Fig. 5, four photographs taken on 8 September 2015 at local noon (during the passage of the main, rather dense dust front) from the roof of a high building (AERONET station) at Limassol to the south and north are presented. The left photographs show the situation during the phase with the heaviest dust load (8 September, around local noon). These pictures are in strong contrast to the photographs taken one day later, when the dust concentration was still high but the horizontal visibility increased already to values of around 8–10 km. By careful inspection of the pictures from 8 September (searching for different pronounced buildings and towers) we estimated the horizontal visibility to be 500–600 m. The visibility measurements performed at three airports in Cyprus are discussed in the next subsection. A visibility of 500 m points to dust extinction coefficients of about 6000 Mm^{-1} according to Eq. (2). If this extremely high extinction coefficient occurred at all heights throughout the lower dust layer up to 1.5 km height, as suggested by the 12 UTC radiosonde RH profile, we end up with AOTs of close to 9. Even if we assume a lower average extinction value of 4000 Mm^{-1}, the AOT would be close to 6. Such huge dust optical depths indicate column dust loads of 10–15 g/m^2. In the upper layer, the AOT was significantly lower with values around 0.5 or less as the lidar observations on 7 and 9–11 September indicate. This is consistent with the fact that the higher parts of the Troodos mountains remained always visible, even on 8 September in Fig. 1.

Figure 4 also shows height profiles of the dust outbreaks simulated with the RAMS-ICLAMS model (Regional Atmospheric Modeling System / Integrated Community Limited Area Modeling System) (Cotton et al., 2003; Solomos et al., 2011). Details to this simulations are given in the follow-up paper (Solomos et al., 2016, in preparation). Dust profiles for arrival times in the evening of 7 September and local noon of 8 September 2015 are shown. The regional model (simulation with 20 km horizontal

resolution) clearly underestimates the dust load. As explained in detail by Solomos et al. (paper in preparation) the event seems to be the result of two meteorological processes. A thermal low formed over Syria on 6 September 2015 associated with strong cloud convection and provided favorable conditions for the generation of a haboob along the borders between Iraq-Iran-Turkey-Syria on 7 September 2015. Atmospheric density currents evolved and propagated towards the Mediterranean and pushed the pre-existing elevated dust layers towards the Mediterranean Sea. The main reasons that most dust prediction models (including RAMS in regional modeling configuration with too low horizontal resolution to resolve cloud convection processes) did not capture this episode are possibly related to the lack of sufficient physics package to describe the feedback of clouds on dust mobilization and the lack of sufficient (cloud resolving) model resolution. A detailed discussion is given in the follow-up study (Solomos et al., paper in preparation).

3.2 Dust optical properties and mass concentrations: surface and profile observations

Figure 6a shows time series of AOT retrieved from daily MODIS observations for four coastal sites from Risocarpaso at the most eastern tip of Cyprus to Pafos, which is approximately 250 km southwest of Risocarpaso. In addition, the AOT time series for the capital city Nicosia is shown. The mean AOT values for areas with radius of 50 km around these cities are presented. Only values that passed a quality check (QAC) are included in the averaging. These are level-2 single pixel AOT(550 nm) measurements with a QAC flag of 3 and a QAC flag greater than 0 were used over land and over ocean, respectively. The maximum retrievable AOT is 5.0. Many of the individual validated (pixel) AOT values were set to 5.0 (although the true value was larger). For Fig 6, we used all validated data points in the averaging. Therefore, the area mean values for 8 September (Julian day 251) have to be interpreted with caution. Furthermore, as outlined in the foregoing section, the uncertainty in the retrievable AOT values is about $0.05 \pm 0.15 \times$AOT.

One can see that the AOT at Limassol was around and above 1.0 for four days (8-11 September). We speculate that the maximum AOT was in the range of 6-9 on 8 September 2015, as discussed above. Our lidar observations on 7 and 9-10 September indicate that the AOT contribution of the second layer above 1.5 km height was always of the order of 0.5.

According to MODIS, the AOT ranged from 0.85–1.7 on 9 September 2015, 1.2–2.1 on 10 September, and 1.1–1.4 on 11 September over southern Cyprus (Larnaca, Limassol). The AOT was considerably lower at Pafos on 9–10 September, 70 km west of Limassol, with values of 0.4 and 0.3–0.7, respectively. In comparison, our lidar observations (taken about 6–11 hours after the daily MODIS observations) indicate AOTs of 0.5-0.6 on 9 September (MODIS, Limassol, 0.85, Pafos 0.4), 0.7–0.75 on 10 September (MODIS, Limassol 1.2, Pafos, 0.3–0.7), and around 0.85 on 11 September (MODIS, Limassol, 1.1, Pafos, 0.8). On 12 September 2015, all three stations showed significantly reduced dust loads with AOT values from 0.3–0.8 derived from the MODIS observations. In this context it should be mentioned that the relative humidity was always $<30\%$, $<40\%$, $<50\%$ within the lowermost one kilometer, up the top of the lower dust layer, and up to the top of the upper dust layer, respectively, on 7–11 September, so that effects of aerosol particle growth by water uptake on the observed AOT values can be neglected. The impact of anthropogenic particles and marine particle may have been of the order of 0.05–0.15 and 0.03–0.05 on the total AOT at 500 nm during the dust period.

Figure 6b shows that the Ångström exponent (AE), which describes the wavelength dependence of AOT (for the visible wavelength range from 510–670 nm), dropped from typical values of 1.0–1.5 for mixtures of anthropogenic aerosol and marine particles (and some local dust) to values around 0.3 during the dust period (ignoring the low AE values on 8 September which are mostly based on biased AOT values).

Figure 6c presents the surface observations of PM_{10} concentrations from 6-14 September 2015. Hourly mean values for five sites across Cyprus are shown. The uncertainty in this values is of the order of 50%. The maximum hourly mean dust mass concentration at Limassol was close to 8000 μg/m^3 on 8 September. The quality-assured daily mean values were 2900 μg/m^3 (Larnaca), 1500 μg/m^3 (Limassol), and 500 μg/m^3 (Pafos) on 8 September, 2015.

The PM_{10} observations may have underestimated the total-suspended-particle (TSP) mass concentration. Kandler et al. (2009) showed that the TSP mass concentration can be an order or even two orders of magnitude larger than the respective PM_{10} value during haze periods and density current-induced dust fronts. TSP mass concentrations of up 300000 μg/m^3 were observed in southeastern Morocco, close to the Sahara, and simultaneously, the PM_{10} values was of the order of 3000 μg/m^3 only. Particles with diameters >10 μm often accounted for more than 90% of the total airborne aerosol mass in southeastern Morocco. At Cabo Verde, after long range transport of dust over 1000–3000 km, the TSP-to-PM_{10} particle mass concentration ratio was found to be mostly between 1.2–1.5 Kandler et al. (2011).

To check to what extend the PM_{10} dust observations underestimated the TSP mass concentration during these extreme dust conditions of 8 September 2015, we analyzed visibility observations at three airports in southern Cyprus. According to Eq. (2) in Sect. 2.4, the visibility is directly related to the particle extinction coefficient, which in turn is highly correlated with the particle volume and mass concentration. The relative uncertainty in the derived mass concentration is estimated to be about 30-40%, provided the visibility is available with an uncertainty of 20-30%.

Figure 7 shows time series of visibility and corresponding extinction coefficient. All three stations show visibilities in the range from 200-750 m from 5:00 to 20:00 (Larnaca), 6:00–14:00 (Limassol), and 10:00–14:00 (Pafos). The lowest visibilities of 200–300 m values in the Limassol area were observed at Acrotiri airport (about 10 km southwest of the Limassol lidar station) from 8–9 UTC, when the photographs in Figure 5 were taken. The corresponding particle extinction and mass concentration values for Acrotiri are 9000–15000 Mm^{-1} and 15000–25000μg/m^3, respectively. As mentioned in Sect. 2, marine and anthropogenic haze may have contribute to the total aerosol extinction coefficient by 50–100 Mm^{-1} each so that their contribution to observed extinction values exceeding 2000 or 3000 Mm^{-1} can be ignored in the following discussion and retrievals.

The visibility of 500 m is related to peak particle extinction coefficient of 6000 Mm^{-1} and correspondingly to a peak TSP mass concentration of 10000 μg/m^3. This peak TSP value is about a factor of 1.25-1.3 higher than the in situ measured maximum hourly mean PM_{10} value of around 7600 μg/m^3. This can be regarded as an excellent agreement when taking the study of Kandler et al. (2011) on the relationship between TSP mass versus PM_{10} into consideration.

However, if we compare the quality-assured daily mean in-situ measured PM_{10} values for Larnaca (2900 μg/m^3), Limassol (1500 μg/m^3), and Pafos (500 μg/m^3) on 8 September 2015, with the respective daily mean TSP mass concentrations (calculated from MOR values measured every hour), we find visibility-related daily mean TSP mass concentrations of 3600 μg/m^3

(Laranca), 2075 μg/m^3 (Acritori, Limassol), and 1600 μg/m^3 (Pafos), which are a factor of 2.5 (Larnaca), 2.8 (Limassol), and 6.4 (Pafos) higher than the in-situ measured PM_{10} daily means. These very high (and to our opinion unrealistic) factors of 2.5–6.4 may be caused by a wrong volume-to-extinction conversion factor $c_{v,d} = v_d/\sigma_d$ (a factor of 2 too high) in Eq. (3), or by a wrong visibility estimations (roughly a factor of 2 too high) at these unusual very dust conditions. The volume-to-extinction conversion factor is 0.64×10^{-12}Mm (as discussed in Sect. 2.1). A value around 0.32×10^{-12}Mm points to conditions with dominating fine-mode dust (Mamouri and Ansmann, 2016). At strong dust outbreak conditions we expect the opposite, namely that coarse-mode dust particles dominate the measured optical effects so that the volumne-to-extinction conversion factor higher than 0.64×10^{-12}Mm.

The next days showed steadily decreasing near-surface dust mass concentrations. The daily mean PM_{10} mass concentration decreased from 2900 μg/m^3 (8 September) to 1000, 500, and 200 μg/m^3 on the following day (9–11 September) at Larnaca, and from 1500 μg/m^3 (8 September) to 500, 200, and 200 μg/m^3 at Limassol on 9–11 September. This steady decrease of the near-surface dust mass concentration was not observed for the total column (see discussion of MODIS and lidar-derived AOTs above) which remained almost constant from 9–11 September.

The highlight of the observations are our lidar observations of the vertical layering of the dust particles. Such profile observations are indispensable in the verification of modeling results and the reliability of model-based dust outbreak studies as a whole. Figure 3 provides an overview of the main dust layering features and indicated a two-layer structure of the advected dust plumes which pointed to two different air mass transport regimes and thus two dust source regions.

In Fig. 8, profiles of particle backscatter and extinction coefficients at 532 nm, the corresponding extinction-to-backscatter ratio (lidar ratio), and the particle linear depolarization ratio at 532 nm for each of the four evenings on 7 and 9–11 September are given. 1-hour to 3-hour mean profiles provide an overview of the main features of the dust optical properties. The backscatter coefficients are obtained with high vertical resolution (signal smoothing window length of 195 m) and show best the layer structures. The profiles of the particle backscatter coefficient and the particle linear depolarization ratio are trustworthy down to 100 m above ground as the comparison with the surface in situ observations (PM_{10} measurements, visbility/extinction observations) corroborate which will be discussed below. The extinction coefficients and corresponding lidar ratios are calculated from smoothed Raman signal profiles (375m smoothing length).

The particle extinction coefficients reached values of 1300 Mm^{-1} in the lower layer and were around 350 Mm^{-1} in the second layer on 7 September. Another pronounced dust front caused extinction coefficients up to 550 Mm^{-1} in an elevated layer between 1000 and 2500 m height on 10 September 2015. The lidar ratios at 532 nm were 35-42 sr in the dust layers on 7 and 10 September, 45-60 sr on 9 September, and 50-60 sr on 11 September. Values of 35–45 sr are typical for desert dust from Middle East dust sources (Mamouri et al., 2013; Nisantzi et al., 2015). Larger lidar ratios on 9 and 11 September indicate a mixture of dust and anthropogenic haze. As mentioned above, hygroscopic particle growth effects on the oberved optical properties can be neglected.

The particle linear depolarization ratio assumed typical dust values of 0.25-0.32 (7 and 10 September) in the dense dust layers. These values clearly indicate the dominance of mineral dust in these layers. The decrease towards values of 0.20-0.25 on 9 and 11 September reflects the increasing impact of anthropogenic haze on the optical properties of the advected air masses.

The linear depolarization ratio dropped to values clearly below 0.2 in the lowermost 300–500 m thick marine boundary layer over Limassol and was around 0.1–0.15 at 100 m above ground. Such low depolarization ratios indicate that anthropogenic pollution contributed to more than 50% to the overall total particle backscattering and extinction coefficients and to 30–50% to the particle mass concentration in the city. This fact has to be kept in mind when comparing PM_{10} mass concentrations with the mass concentrations derived from the lidar profiles at heights below about 300–500 m.

The backscatter and extinction profiles and the lidar ratio information allow us to estimate the AOT in the lower dust layer (partly from the backscatter coefficients) and to termine the AOT at 532 nm in the upper dust layer, from the extinction profile. We estimated the extinction values in the vertical range without extinction measurements (in the lowermost about 800 m) by multiplying the backscatter coefficients with a lidar ratio of 50 sr which is higher than a pure-dust lidar ratio and takes the influence of anthropogenic pollution (lidar ratios of 60-80 sr) into account. On 7 September, the 532 nm AOT for the lower layer (0–1.7 km height) was 1.2, and 0.5 for the upper layer from 1.7–3.5 km. On 9 September, the 532 nm AOT decreased strongly from the record-breaking values >5.0 on 8 September to values around 0.5 with an AOT around 0.35 for the lowermost 1.2 km height region and 0.2 for the upper dust layer from 1.2–3.0 km height. In contrast to the evening lidar observations, the morning MODIS data revealed still an AOT of 0.8-1.0 on 9 September. Another dense dust outbreak plume then reached Cyprus on 10 September. The daytime AOT (MODIS) for Limassol showed a slight increase to 1.0–1.2, the lidar observed an overall AOT of 0.7–0.8 (as three hour average) in the nighttime of 10 September 2015. The lower dust layer (up to 1 km height) contributed about 0.2–0.3 and the upper layer (1–3 km) around 0.5 to the total AOT. A more vertically homogeneous dust extinction backscatter and extinction profiles were observed on 11 September with an AOT of around 0.6 for the lower part (0–1.8 km height) of the dust layer and an AOT of about 0.25 for the upper part from 1.8-4.2 km height. MODIS AOT values on 11 September were still around 1.0 (for all stations Larnaca, Limassol, Pafos). Thus a good agreement between MODIS and lidar observations was found for this final dust day.

We also studied to what extent the lidar backscatter coefficients and the estimated extinction values close to the ground are reliable. Visibility observations yield values for the meteorological optical range of around 8–10 km in the evening of 9 September, which corresponds to particle extinction coefficients of 300–375 Mm^{-1}. The lidar measurements indicate backscatter coefficients of 6 Mm^{-1} sr^{-1} close to the surface on 9 September, and thus extinction coefficients of 275 Mm^{-1} (by multiplying the backscatter coefficient with a lidar ratio of 45 sr, representing dust-dominated conditions) to 330 Mm^{-1} (for a lidar ratio of 55 sr, representing urban-haze-dominating conditions). The good agreement indicates that urban haze controls the surface-near aerosol extinction coefficient which is corroborated by the low particle linear depolarization ratio of 0.08-0.15 at heights <500 m.

An overview of the vertical dust mass distribution, observed in the evenings of 7, 9, 10, and 11 September 2015, is given in Fig. 9. In Eq. (1), we used the dust lidar ratio of 40 sr. After the first very dense dust plumes on 7-8 September, another dense dust plume crossed Limassol in the evening of 10 September and the dust mass concentrations was again high with values close to 800 $\mu g/m^3$ in the center of the elevated layer from 1000-2500 m height. The two-layer structure vanished on 11 September. Only one layer extending from the surface up to 4.2 km height was observed. In terms of column dust mass concentrations we

obtained values of 1.9 g/m^2 (for 7 September in Fig. 9), 0.35 g/m^2 (9 September), 0.95 g/m^2 (10 September), and 0.6 g/m^2 (11 September). AOTs of 6–9 as estimated for the peak dust front on 8 September indicate peak column dust loads of 10–15 g/m^2.

Regarding the quality of the lidar-derived TSP mass concentrations close to the ground, we compared the lidar data with respective PM_{10} observations (mean values for the lidar measurement periods in Fig. 9). The Limassol evening PM_{10} values (considering dust and aerosol pollution) were 55 μg/m^3 (7 September), 120 μg/m^3 (9 September), 125 μg/m^3 (10 September), and 165 μg/m^3 (11 September). The respective lidar-derived total aerosol mass concentrations were 65 μg/m^3 (7 September), 180 μg/m^3 (9 September), 125 μg/m^3 (10 September), and 290 μg/m^3 (11 September). The uncertainties are roughly 30% for the lidar mass values and 50% for hourly-mean PM_{10} values. Again, good agreement is obtained keeping the uncertainties in the derived values into account. Inhomogeneous downward mixing of dust and horizontal inhomogeneities in the dust and urban pollution distributions may have also contributed to the differences. Note, that Fig. 9 only shows the dust-related mass concentrations. The contribution of urban and marine aerosol to the TSP mass concentration was of the order of 20–30 μg/m^3 (7 and 10 September) and 40–50 μg/m^3 (9 and 11 September 2015).

4 Conclusions

A record-breaking dust storm over the Eastern Mediterranean in September 2015 has been documented and discussed based on satellite, lidar, and in situ aerosol observations in the Cyprus area. We were able to provide a consistent picture of this dust event in terms of a variety optical and microphysical, and dust layering properties obtained by means of very different in situ and remote sensing observational techniques and retrieval approaches. The highlight of the study were the vertically resolved lidar observations. The presented documentation of an extreme dust storm based on state-of-the-art lidar, satellite and in situ observations is a valuable contribution to the literature dealing with long-range transport of dust, forecasting of dust outbreaks, and the research on the relationship between meteorological conditions and dust emission strength.

Such unique events may take place once in a decade or even less frequently and are thus obviously linked to unique meteorological constellations. The documentation of extremely seldom dust storms with vertical, horizontal and temporal resolution (in this article) in combination with advanced atmospheric modeling covering cloud evolution, development of thunderstorm, density currents, dust mobilization and dust transport (in the follow-up article) will certainly lead to an improved understanding of the evolution of dust storms at extreme meteorological conditions. The modeling studies will further reveal what kind of modeling infrastructure is required to resolve even small-scale hot spots of dust mobilization phenomena in order to improved dust forecasting in general.

Another concluding remark deals with the need of a dust lidar network around the main desert areas, e.g. in the Europe-Africa-Asia region from the Sahara, over the Middle East deserts to the desert regions in central, southern and eastern Asia. Continuously operated lidars would be an ideal supplement to dust forecast dust model efforts with the potential goal to assimilate the lidar products in to the forecast models. As demonstrated in this article, modern polarization lidars allow us to separate dust and non dust optical properties and to quantify the dust-related particle extinction coefficient and mass concentration in the vertical profile profile with an uncertainty of 20-30%.

Acknowledgements. The authors thank the Eratosthenes Research Center of CUT for support. R.-E. M. would like to thank CUT's library for the financial support within Cyprus University of Technology Open Access Author Fund. The authors acknowledge support through the following projects and research programs: ACTRIS Research Infrastructure (EU H2020-R&I) under grant agreement no. 654169, BEYOND (Building Capacity for a Centre of Excellence for EO-based monitoring of Natural Disasters, FP7-REGPOT-2012-2013-1) under grant agreement no. 316 210, BACCHUS (impact of Biogenic vs. Anthropogenic emissions on Clouds and Climate: towards a Holistic UnderStanding, EU FP7-ENV-2013) under grant agreement project number 603445, and GEO-CRADLE (EU H2020 R&I) under grant agreement No 690133. The authors are very thankful to the Air Quality Department (Department of Labour Inspection, DLI) for establishing and maintaining the air quality stations of Republic of Cyprus, and Dr Chrysanthos Savvidis (DLI) for providing quality–assured PM_{10} daily means. We further thank Dr Filippos Tymvios from the Department of Meteorology (DoM) of Cyprus for the visibility observations. The authors gratefully acknowledge the NOAA Air Resources Laboratory (ARL) for the provision of the HYSPLIT transport and dispersion model as well for the provision of Global Data Assimilation System (GDAS) data used in this publication. The Terra/MODIS Aerosol Daily datasets were acquired from the Level-1 & Atmosphere Archive and Distribution System (LAADS) Distributed Active Archive Center (DAAC), located in the Goddard Space Flight Center in Greenbelt, Maryland (https://ladsweb.nascom.nasa.gov/). We acknowledge the use of data products or imagery from the Land, Atmosphere Near real-time Capability for EOS (LANCE) system operated by the NASA/GSFC/Earth Science Data and Information System (ESDIS) with funding provided by NASA/HQ.

References

Amiridis V., Balis, D., Kazadzis, S., Giannakaki, E., Papayannis, A., and Zerefos, C.: Four years aerosol observations with a Raman lidar at Thessaloniki, Greece, in the framework of European Aerosol Research Lidar Network (EARLINET), J. Geophys. Res., 110, D21203, doi:10.1029/2005JD006190, 2005.

Ansmann, A., Tesche, M., Seifert P, Groß, S., Freudenthaler, V., Apituley, A., Wilson, K. M., Serikov, I., Linné, H., Heinold, B., Hiebsch, A., Schnell, F., Schmidt, J., Mattis, I., Wandinger, U., and Wiegner, M.: Ash and fine–mode particle mass profiles from EARLINET-AERONET observations over central Europe after the eruptions of the Eyjafjallajökull volcano in 2010, J. Geophys. Res., 116, D00U02, doi:10.1029/2010JD015567, 2011.

Ansmann, A., Seifert, P., Tesche, M., and Wandinger, U.: Profiling of fine and coarse particle mass: case studies of Saharan dust and Eyjafjallajökull/Grimsvötn volcanic plumes, Atmos. Chem. Phys., 12, 9399–9415, doi:10.5194/acp-12-9399-2012, 2012.

Cotton W. R., Pielke Sr., R. A., Walko, R. L., Liston, G. E., Tremback, C. J., Jiang, H., McAnelly, R. L., Harrington, J. Y., Nicholls, M. E., Carrio, G. G., and McFadden, J. P.: RAMS 2001: Current status and future directions, Meteor. Atmos. Phys., 82, 5-29, 2003

Georgoulias, A. K., Alexandri, G., Kourtidis, K. A., Lelieveld, J., Zanis, P., Pöschl, U., Levy, R., Amiridis, V., Marinou, E., and Tsikerdekis, A.: Spatiotemporal variability and contribution of different aerosol types to the Aerosol Optical Depth over the Eastern Mediterranean, Atmos. Chem. Phys. Discuss., doi:10.5194/acp-2016-401, in review, 2016.

Gkikas, A., Basart, S., Hatzianastassiou, N., Marinou, E., Amiridis, V., Kazadzis, S., Pey, J., Querol, X., Jorba, O., Gassó, S., and Baldasano, J. M.: Mediterranean intense desert dust outbreaks and their vertical structure based on remote sensing data, Atmos. Chem. Phys., 16, 8609-8642, doi:10.5194/acp-16-8609-2016, 2016.

Guerrero-Rascado, J. L., Olmo, F. J., Avilés-Rodríguez, I., Navas-Guzmán, F., Pérez-Ramírez, D., Lyamani, H., and Alados Arboledas, L.: Extreme Saharan dust event over the southern Iberian Peninsula in september 2007: active and passive remote sensing from surface and satellite, Atmos. Chem. Phys., 9, 8453-8469, doi:10.5194/acp-9-8453-2009, 2009.

Heinold, B., Tegen, I., Esselborn, M., Kandler, K., Knippertz, P., Müller, D., Schladitz, A., Tesche, M., Weinzierl, B., Ansmann, A., Althausen, D., Laurent, B., Massling, A., Müller, T., Petzold, A., Schepanski, K., and Wiedensohler, A.: Regional Saharan dust modelling during the SAMUM 2006 campaign Tellus B, 61, 307–324, doi:10.1111/j.1600-0889.2008.00387.x, 2009

Heinold, B., Tegen, I., Schepanski, K., Tesche, M., Esselborn, M., Freudenthaler, V., Groß, S., Kandler, K., Knippertz, P., Müller D., Schladitz, A., Toledano, C., Weinzierl, B., Ansmann, A., Althausen, D., Müller, T., Petzold, A., and Wiedensohler, A.: Regional modelling of Saharan dust and biomass-burning smoke: Part I: Model description and evaluation Tellus B, 63, 781–799, doi:10.1111/j.1600-0889.2011.00570.x, 2011.

Holben, B. N., Eck, T. F., Slutsker, I., Tanré, D., Buis, J. P., Setzer, A., Vermote, E., Reagan, J. A., Kaufman, Y. J., Nakajima, T., Lavenu, F., Jankowiak, I., and Smirnov, A.: AERONET – A federated instrument network and data archive for aerosol characterization, Remote Sens. Environ., 66, 1–16, 1998.

Horvath, H.: On the applicability of the Koschmieder visibility formula, Atmos. Env, 5, 177-184, 1971.

Horvath, H., and Noll, K. E.: The relationship between atmospheric light scattering coefficient and visbility, Atmos. Env., 3, 543-550, 1969.

Kandler, K., Schütz, L., Deutscher, C., Ebert, M., Hofmann, H., Jäckel, S., Jaenicke, R., Knippertz, P., Lieke, K., Massling, A., Petzold, A., Schladitz, A., Weinzierl, B., Wiedensohler, A., Zorn, S., and Weinbruch, S.: Size distribution, mass concentration, chemical and mineralogical composition and derived optical parameters of the boundary layer aerosol at Tinfou, Morocco, during SAMUM 2006, Tellus B, 61, 32–50, doi:10.1111/j.1600-0889.2008.00385.x, 2009.

Kandler, K., Schütz, L., Jäckel, S., Lieke, K., Emmel, C., Müller-Ebert, D., Ebert, M., Scheuvens, D., Schladitz, A., Segvić, B., Wiedensohler, A., and Weinbruch, S.: Ground-based off-line aerosol measurements at Praia, Cape Verde, during the Saharan Mineral Dust Experiment: microphysical properties and mineralogy, Tellus B, 63, 459–474, doi:10.1111/j.1600-0889.2011.00546.x, 2011.

Knippertz, P., Deutscher, C., Kandler, K., Muller, T., Schulz, O., and Schutz L.: Dust mobilization due to density currents in the Atlas region. Observations from the Saharan Mineral Dust Experiment 2006 field campaign, J. Geophys. Res., 112, D21109, doi:10.1029/2007JD008774, 2007.

Koschmieder, H.: Theorie der horizontalen Sichtweite, Beiträge zur Physik der freien Atmosphäre, 12, 33–53, 1924.

Levy, R. C., Remer, L. A., Kleidman, R. G., Mattoo, S., Ichoku, C., Kahn, R., and Eck, T. F.: Global evaluation of the Collection 5 MODIS dark-target aerosol products over land, Atmos. Chem. Phys., 10, 10399-10420, doi:10.5194/acp-10-10399-2010, 2010.

Levy, R. C., Mattoo, S., Munchak, L. A., Remer, L. A., Sayer, A. M., Patadia, F., and Hsu, N. C.: The Collection 6 MODIS aerosol products over land and ocean, Atmos. Meas. Tech., 6, 2989-3034, doi:10.5194/amt-6-2989-2013, 2013.

Mamouri, R. E., Papayannis, A., Amiridis, V., Müller, D., Kokkalis, P., Rapsomanikis, S., Karageorgos, E. T., Tsaknakis, G., Nenes, A., Kazadzis, S., and Remoundaki, E.: Multi-wavelength Raman lidar, sun photometric and aircraft measurements in combination with inversion models for the estimation of the aerosol optical and physico-chemical properties over Athens, Greece, Atmos. Meas. Tech., 5, 1793-1808, doi:10.5194/amt-5-1793-2012, 2012.

Mamouri, R. E., Ansmann, A., Nisantzi, A., Kokkalis, P., Schwarz, A., and Hadjimitsis, D.: Low Arabian dust extinction-to-backscatter ratio, Geophys. Res. Lett., 40, 4762–4766, doi:10.1002/grl.50898, 2013.

Mamouri, R. E. and Ansmann, A.: Fine and coarse dust separation with polarization lidar, Atmos. Meas. Tech., 7, 3717-3735, doi:10.5194/amt-7-3717-2014, 2014.

Mamouri, R. E. and Ansmann, A.: Estimated desert-dust ice nuclei profiles from polarization lidar: methodology and case studies, Atmos. Chem. Phys., 15, 3463-3477, doi:10.5194/acp-15-3463-2015, 2015.

Mamouri, R. E. and Ansmann, A.: Fine and coarse dust separation with polarization lidar: Extended methodology for multiple wavelengths, in preparation, to be submitted to the AMT/ACP SALTRACE Special Issue, 2016.

Mona, L., A. Amodeo, M. Pandolfi, and G. Pappalardo, Saharan dust intrusions in the Mediterranean area: Three years of Raman lidar measurements, J. Geophys. Res., 111, D16203, doi:10.1029/2005JD006569, 2006.

Mona, L., Papagiannopoulos, N., Basart, S., Baldasano, J., Binietoglou, I., Cornacchia, C., and Pappalardo, G.: EARLINET dust observations vs. BSC-DREAM8b modeled profiles: 12-year-long systematic comparison at Potenza, Italy, Atmos. Chem. Phys., 14, 8781-8793, doi:10.5194/acp-14-8781-2014, 2014.

Müller, D., Heinold, B., Tesche, M., Tegen, I., Althausen, D., Alados-Arboledas, L., Amiridis, V., Amodeo, A., Ansmann, A., Balis, D., Comerion, A., D'Amico, G., Gerasopoulos, E., Guerrero-Rascado, J. L., Freudenthaler, V., Giannakaki, E., Heese, B., Iarlori, M., Knippterz, P., Mamouri, R. E., Mona, L., Papayannis, A., Pappalardo, G., Perrone, R.-M., Pisani, G., Rizi, V., Sicard, M., Spinelli, N., Tafuro, A., and Wiegner, M.: EARLINET observations of the 14–22-May long-range dust transport event during SAMUM 2006: validation of results from dust transport modelling, Tellus B, 61, 325–339, doi:10.1111/j.1600-0889.2008.00400.x, 2009.

Nisantzi, A., Mamouri, R. E., Ansmann, A., and Hadjimitsis, D.: Injection of mineral dust into the free troposphere during fire events observed with polarization lidar at Limassol, Cyprus, Atmos. Chem. Phys., 14, 12155-12165, doi:10.5194/acp-14-12155-2014, 2014.

Nisantzi, A., Mamouri, R. E., Ansmann, A., Schuster, G. L., and Hadjimitsis, D. G.: Middle East versus Saharan dust extinction-to-backscatter ratios, Atmos. Chem. Phys., 15, 7071-7084, doi:10.5194/acp-15-7071-2015, 2015.

Papayannis, A., Amiridis, V., Mona, L., Tsaknakis, G., Balis, D., Bösenberg, J., Chaikovski, A., De Tomasi, F., Grigorov, I., Mattis, I., Mitev, V., Müller, D., Nickovic, S., Pérez, C., Pietruczuk, A., Pisani, G., Ravetta, F., Rizi, V., Sicard, M., Trickl, T., Wiegner, M., Gerding, M., Mamouri, R. E., D'Amico, G., and Pappalardo, G.: Systematic lidar observations of Saharan dust over Europe in the frame of EARLINET (2000–2002), J. Geophys. Res., 113, D10204, doi:10.1029/2007JD009028, 2008.

Papayannis, A., Mamouri, R. E., Amiridis, V., Kazadzis, S., Pérez, C., Tsaknakis, G., Kokkalis, P., and Baldasano, J. M.: Systematic lidar observations of Saharan dust layers over Athens, Greece in the frame of EARLINET project (2004-2006), Ann. Geophys., 27, 3611–3620, doi:10.5194/angeo-27-3611-2009, 2009.

Pappalardo, G., Amodeo, A., Apituley, A., Comeron, A., Freudenthaler, V., Linné, H., Ansmann, A., Bösenberg, J., D'Amico, G., Mattis, I., Mona, L., Wandinger, U., Amiridis, V., Alados-Arboledas, L., Nicolae, D., and Wiegner, M.: EARLINET: towards an advanced sustainable European aerosol lidar network, Atmos. Meas. Tech., 7, 2389–2409, doi:10.5194/amt-7-2389-2014, 2014.

Solomos, S., Kallos, G., Kushta, J., Astitha, M., Tremback, C., Nenes, A., and Levin, Z.: An integrated modeling study on the effects of mineral dust and sea salt particles on clouds and precipitation, Atmos. Chem. Phys., 11, 873-892, doi:10.5194/acp-11-873-2011, 2011.

Solomos, S., Kallos, G., Mavromatidis, E., and Kushta, J.: Density currents as a desert dust mobilization mechanism, Atmos. Chem. Phys., 12, 11199-11211, doi:10.5194/acp-12-11199-2012, 2012.

Stein, A. F., Draxler, R. R., Rolph, G. D., Stunder, B. J. B., Cohen, M. D., and Ngan, F.: NOAA's HYSPLIT Atmospheric Transport and Dispersion Modeling System. Bull. Amer. Meteorol. Soc., 96, 2059–2077, doi: 10.1175/BAMS-D-14-00110.1, 2015

Tesche, M., Ansmann, A., Müller, D., Althausen, D., Mattis, I., Heese, B., Freudenthaler, V., Wiegner, M., Eseelborn, M., Pisani, G., and Knippertz, P.: Vertical profiling of Saharan dust with Raman lidars and airborne HSRL in southern Morocco during SAMUM, Tellus B, 61, 144–164, doi:10.1111/j.1600-0889.2008.00390.x, 2009a.

Tesche, M., Ansmann, A., Müller, D., Althausen, D., Engelmann, R., Freudenthaler, V., and Groß, S.: Vertically resolved separation of dust and smoke over Cape Verde using multiwavelength Raman and polarization lidars during Saharan Mineral Dust Experiment 2008, J. Geophys. Res., 114, D13202, doi:10.1029/2009JD011862, 2009b.

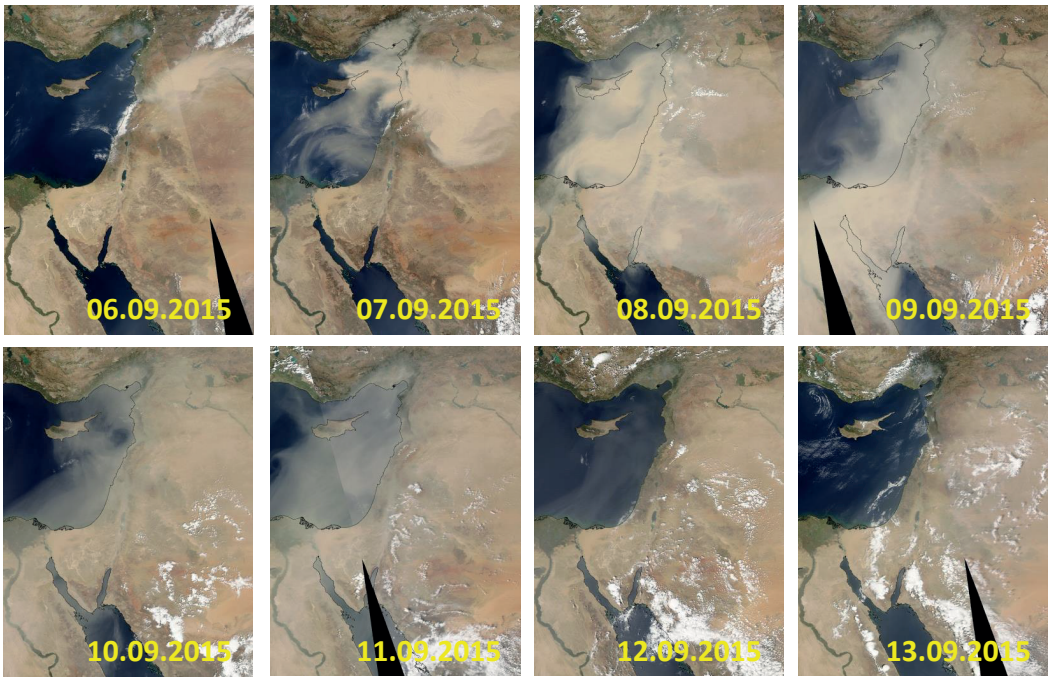

Figure 1. Dust outbreak towards Cyprus in September 2015 as seen from space (AQUA-MODIS, 10:30-11:30 UTC overpasses, 13:30–14:30 EEST, Eastern European Summer Time, http://lance-modis.eosdis.nasa.gov/).

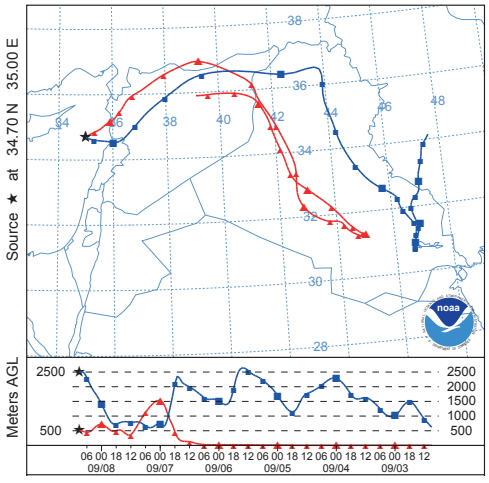

Figure 2. Six–day HYSPLIT backward trajectories (http://www.arl.noaa.gov/HYSPLIT.php) arriving in the Cyprus region at 35°E (about 160 km east of the Limassol lidar station) at 500 m (red, lower dust layer) and 2500 m height (blue, upper dust layer) on 8 September 2015, 09:00 UTC (12:00 EEST)

.

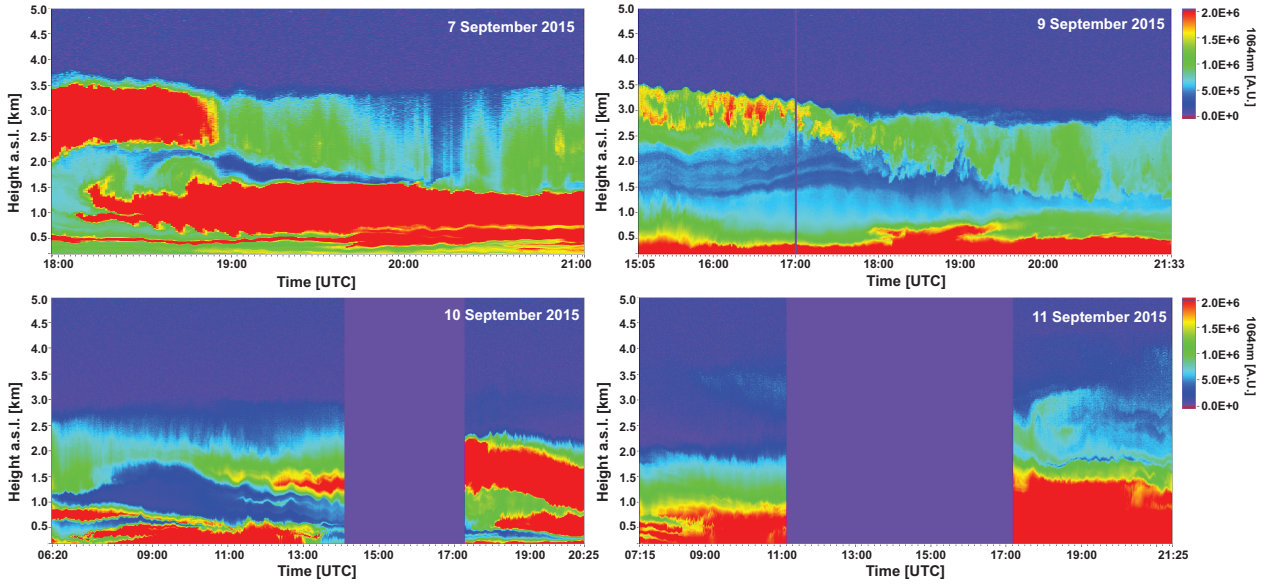

Figure 3. Desert dust layers observed with lidar over the EARLINET station of Limassol, Cyprus, on 7, 9, 10, and 11 September 2015. Range–corrected 1064 nm backscatter signals (in arbitrary units, A. U.) are shown. Red colors indicate dense dust plumes. On 7-10 September, a two-layer structure was observed with dust layers below about 1-1.7 km height and another layer reaching to 2.5-3.7 km height. Local time (EEST) is time in UTC plus 3 hours.

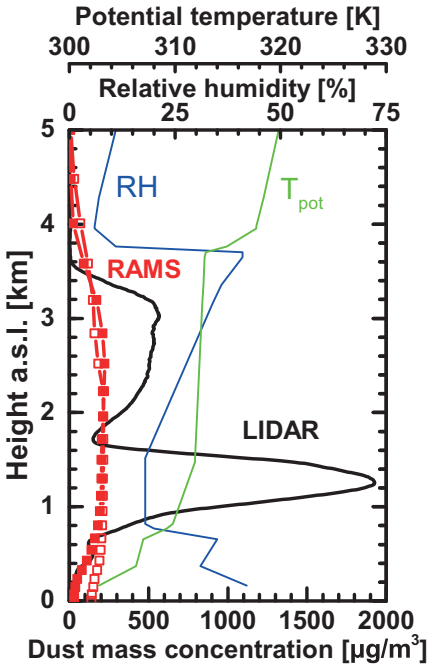

Figure 4. Mean dust mass concentration observed with lidar (thick solid black line) at Limassol on 7 September, 18:00–21:00 UTC, and dust profiles simulated with RAMS (normal run with 20 km horizontal resolution) for Limassol, on 7 September, 18:00 UTC (closed red squares), and 8 September, 9:00 UTC (open squares). Radiosonde observation (launched at the radiosonde station at Athalassa near Nicosia on 8 September 6:00 UTC) of height profiles of potential temperature ($T_{\rm pot}$, thin green curve) and relative humidity (RH, thin blue curve) are in good agreement with the two-layer dust structures observed about 12 hours earlier. The lofted dust layer from 1.7-3.6 km height was well mixed.

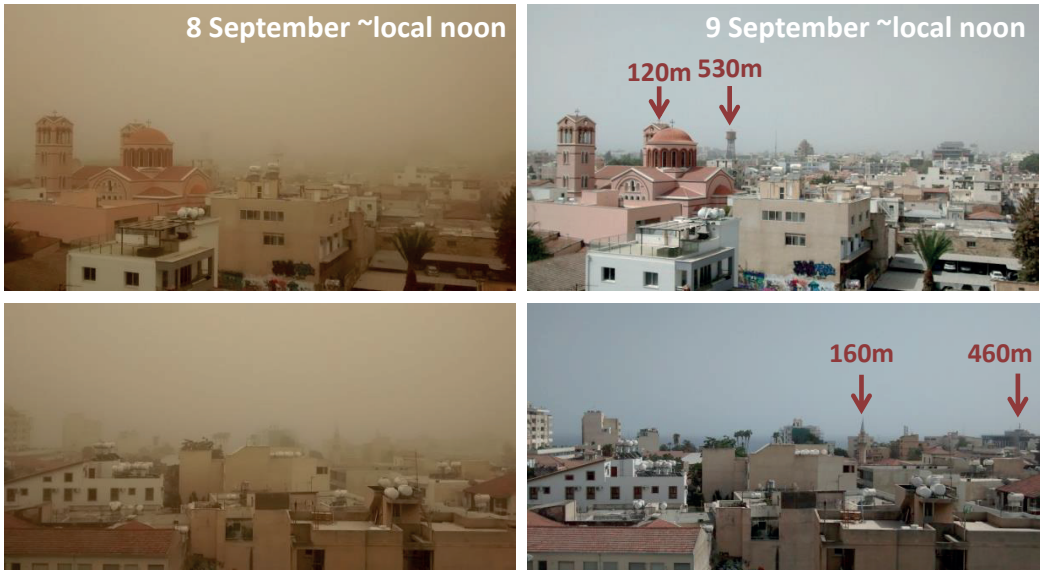

Figure 5. Photographs taken at the roof of a high building (CUT-TEPAK AERONET site) in the city center of Limassol to the north (top) and south (bottom) on 8 September 2015, 8:20-8:30 UTC (left) and on 9 September 2015 (right), again around local noon. The meteorological optical range (or horizontal visibility) was about 500 m on 8 September and higher than 20 km on 9 September 2015. Distances to several towers from the AERONET station are indicated.

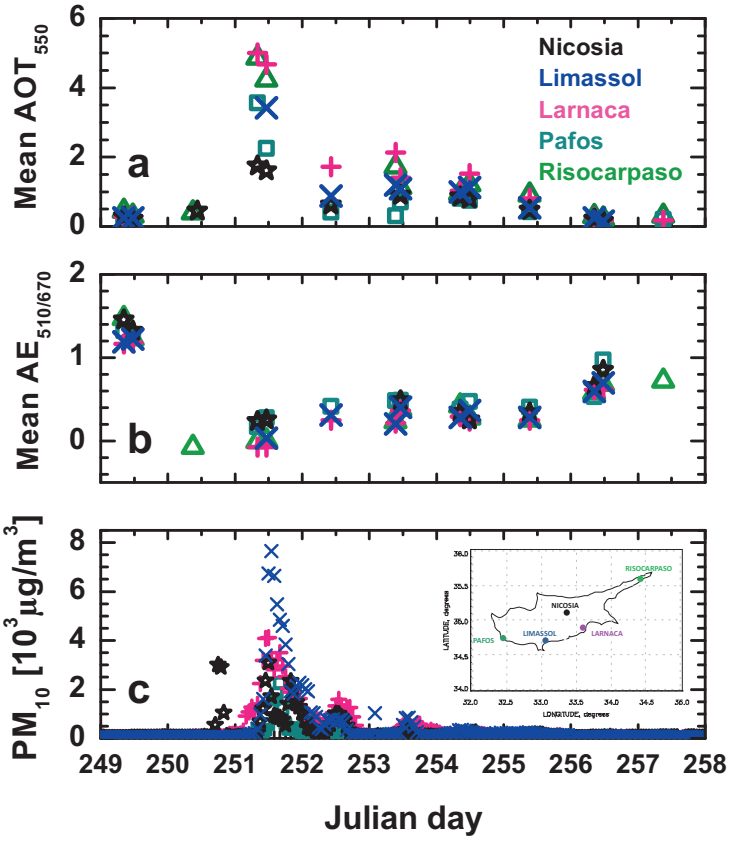

Figure 6. (a) MODIS-derived mean 550 nm aerosol optical thickness (AOT) for five sites in Cyprus for the period from 6-14 September 2015 (Nicosia, stars, Limassol, diagonal crosses, Larnaca, crosses, Pafos, squares, Risocarpaso, triangles, AQUA-MODIS, 10:30-11:30 UTC, and TERRA-MODIS, 8:00–9:00 UTC overpasses), (b) MODIS-derived Ångström exponent (for the 510–670 wavelength range), and (c) hourly mean PM_{10} particle mass concentrations measured at four stations in Cyprus (Nicosia, Limassol, Pafos, Larnaca). The AOTs are determined from all MODIS values within areas with 50 km radius around a given site. MODIS data are available at https://ladsweb.nascom.nasa.gov/data/search.html. The highest retrievable AOT is 5.0. An area-mean values >3.5 are probably biased (underestimation of the true mean AOT, see text). The in situ aerosol observations were performed by the Air Quality Department (Department of Labour Inspection of Cyprus at Limassol) and are available at http://www.airquality.dli.mlsi.gov.cy/. The peak PM_{10} concentration of 7600 μg/m^3 was observed around 9 UTC on 8 September 2015 (Julian day 251)

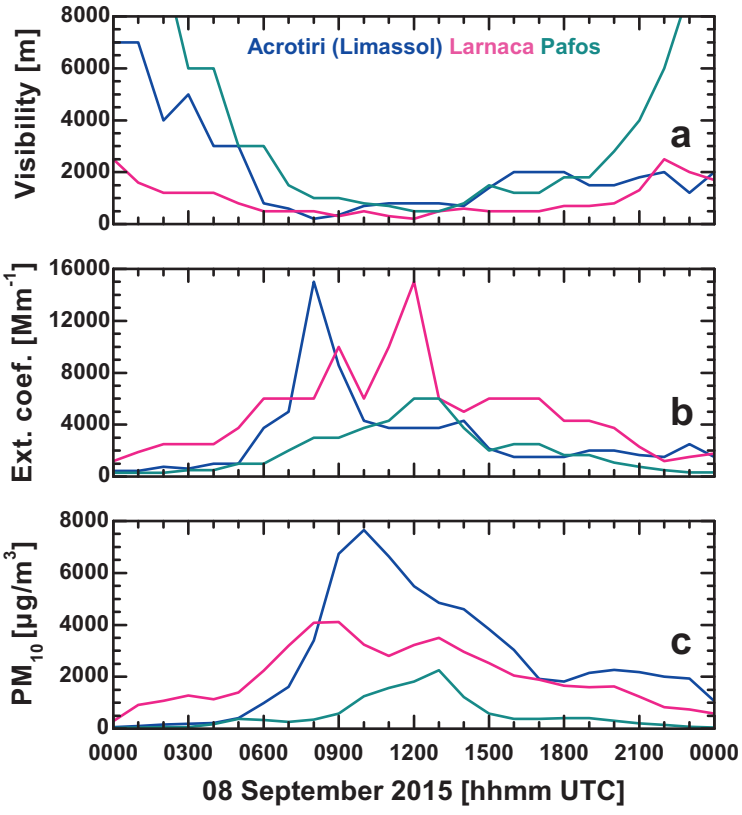

Figure 7. Visibility measured at three airports in southern Cyprus (see map in Fig. 6c) on 8 September 2015, (b) corresponding dust extinction coefficient (by using Eq (2)), and (c) PM_{10} concentrations (same as shown in Fig. 6c). Relative uncertainties in all parameters of of the order of 50%. Dust extinction coefficients of 4000–8000 Mm^{-1} indicate dust mass concentrations of 6600–13300 $\mu g/m^3$.

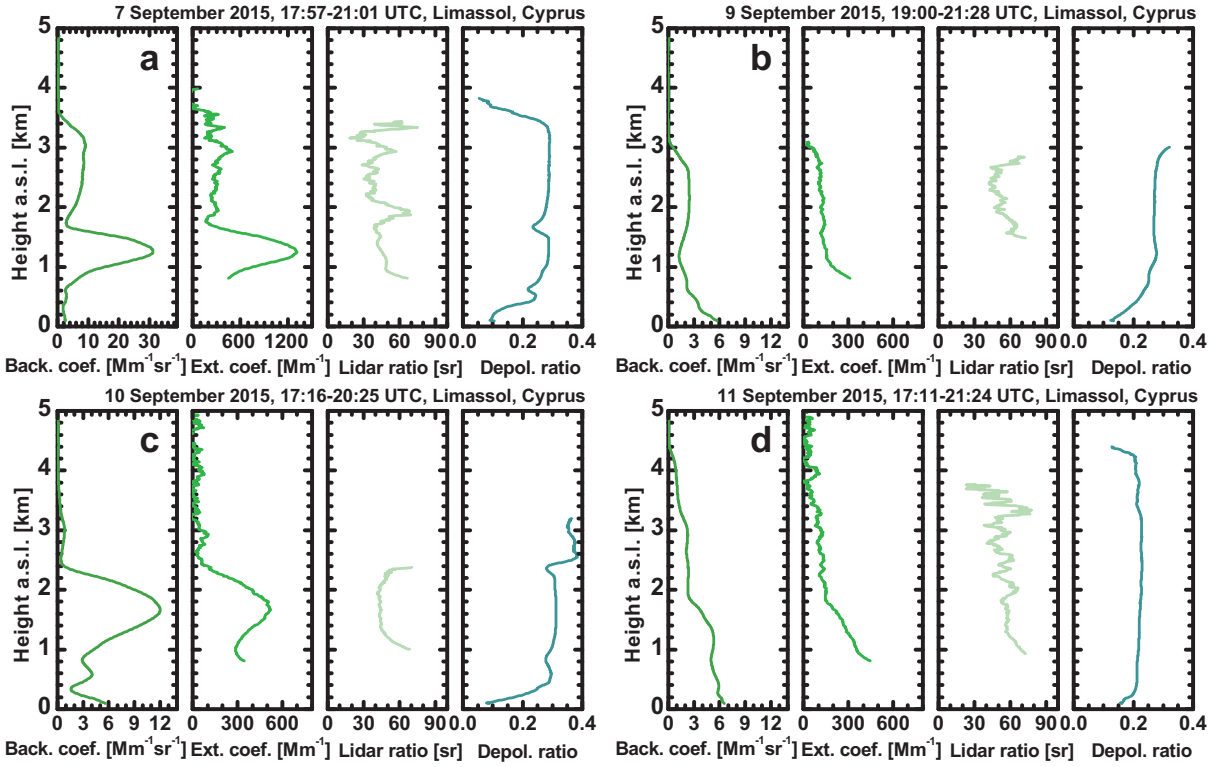

Figure 8. Mean vertical profiles of the 532 nm particle backscatter coefficient, extinction coefficient, lidar ratio, and particle linear depolarization ratio for the observational periods given on top of the panels on 7–11 September 2015. The Raman lidar method is applied. Retrieval uncertainties are of the order of 10% (backscatter coefficient, depolarization ratio), 25% (extinction coefficient), and 30% (lidar ratio).

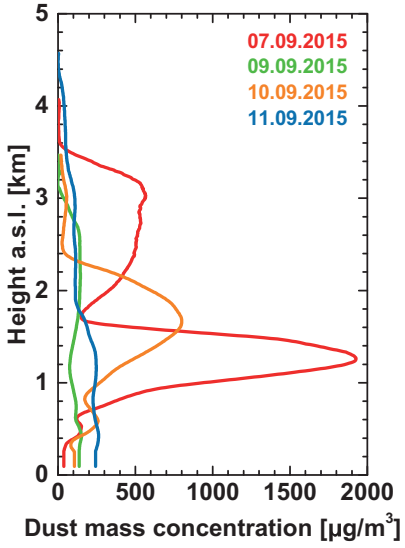

Figure 9. Lidar-derived mean dust mass concentrations for the evening periods (see Fig. 8) of 7 September (18:00–21:00 UTC), 9 September (19:00–21:28 UTC), 10 September (17:16–20:25 UTC), and 11 September (17:11–21:25 UTC). The overall uncertainty in the retrieval of the dust mass concentration is 25%.